Ceramics International **24** (1998) 81–90

PII: S0272-8842(97)00082-X
0272-8842/97 $17.00+.00

The Effect of TiO_2 and MnO_2 on Densification and Microstructural Development of Alumina

H. Erkalfa, Z. Mısırlı & T. Baykara

TUBITAK-Marmara Research Center, Materials and Chemical Technologies Research Institute, Gebze, Turkey

(Received 30 April 1996; accepted 24 September 1996)

Abstract: The effect of MnO_2 and TiO_2 as additives during the densification and microstructural development of Al_2O_3 has been investigated between the temperature range of 1250 and 1550°C. Sintered density, average grain size, microhardness measurements and microstructural features were evaluated to correlate densification with grain growth and second phase formation. Each additive both singly and in combination, was found to increase the final sintered density and microhardness values of the samples. 3 wt% MnO_2 when added with 0.5–3 wt% TiO_2 lowers the sintering temperature to 1250°C. Excessive grain growth and draining of second phase were observed in these samples that were sintered above 1350°C. © 1997 Elsevier Science Limited and Techna S.r.l.

1 INTRODUCTION

Small additions of various oxides, such as MgO, TiO_2, SiO_2, MnO_2, Cr_2O_3, Fe_2O_3, to Al_2O_3 have been shown to influence densification processes by reducing sintering temperature, suppressing or promoting grain growth and allowing sintering to theoretical density. Therefore, a variety of oxides, either singly or in combination, is commonly used in the ceramic industry for various purposes, such as enhancing sintering and to modify the microstructure and mechanical properties. In general, an additive can function either in a solid solution or as a second phase or both by various mechanisms.[1–4] Although many studies on the role of additives in Al_2O_3 have been investigated, there is still a general lack of well-established mechanisms as well as conflicting results.

The influence of TiO_2 and MnO_2 on the sintering of Al_2O_3 was studied both as separate additives and also in combination as TiO_2–MnO_2. Earlier investigations on the sintering of TiO_2 doped Al_2O_3 have shown that an enhanced densification rate was observed during the process. However, there was no indication of a solid solution of 1.0–2.5 mole% TiO_2 in Al_2O_3 when sintering was performed in air. It was argued that the effect of TiO_2 on densification is due to its grain growth enhancement role taking place at grain boundaries.[5,6] In another study, it was revealed that Ti enters Al_2O_3 substitutionally as Ti^{+4} additions increase the concentration of aluminium-ion vacancies, and based on this argument, it is believed that TiO_2 enhances the aluminium-ion diffusion by a vacancy mechanism.[7–9] It was also shown in another quantitative analysis that sintering kinetics were enhanced when TiO_2 was added up to a certain amount above which the sintering rate was found to be levelled off or slightly decreased due to the formation of a second phase at the grain boundary.[10]

The influence of MnO_2, when added singly in the amount of 0.035–7%, was shown to accelerate both the sintering rate and grain growth. Similar to the effect of TiO_2, the sintering rate increases to a maximum level and then decreases as the Mn concentration exceeds 0.3% level due to the formation of a second phase. It was originally proposed that the addition of MnO_2 led to a change in the diffusion mechanism from a grain boundary process to a bulk diffusion process.[11] However, in a more elaborate study, it was suggested that a maximum

sintering rate occurred with addition of 0.3% MnO_2.[12] On the contrary to the bulk diffusion assumptions, it was argued that at concentrations of 0.3% MnO_2 or less, grain boundary diffusion occurred after a certain shrinkage level.

There are very few studies on the simultaneous effects of TiO_2–MnO_2 in Al_2O_3 dealing with the full densification regime and detailed microstructural examination.[13–15] The purpose of this study was to investigate the densification and microstructural development in the TiO_2–MnO_2–Al_2O_3 system in an extensive sintering regime using a varying amount of additives ranging from 0 to 3 wt%. This report also discusses the microhardness values of doped and undoped samples with respect to the microstructural features that developed at different sintering temperatures.

2 EXPERIMENTAL PROCEDURES

Alcoa A 16SG alumina powder with an average particle size of 0.37 μm and reagent-grade $Mn(CH_3COO)_2.4H_2O$ and $TiCl_3$ were used as the starting materials. The acetate of manganese and chloride of titanium can be easily dissolved in water to its ions to yield a homogeneous dispersion.

Alumina suspensions were prepared with the addition of manganese[2] acetate and titanium[3] chloride dissolved in water while its pH adjusted to 2 with HCl. Al_2O_3 was slowly added into the solution while stirring and ultrasonicating to break up the agglomerates. Colloidal suspensions were oven-dried at 110°C and stirred frequently to prevent sedimentation. Dried powders were calcined at 600°C for 1 h in order to obtain insoluble oxides of the additives. Powder compacts were prepared by uniaxial pressing in a steel die to make pellets nominally 2.5 cm in diameter and 0.3 cm in height. Green densities of the pressed samples were measured dimensionally. Undoped and doped samples were sintered at 1250, 1350, 1450 and 1550°C at a heating rate of 10°C min^{-1} for a 1-h sintering hold under the normal furnace atmosphere and cooled at the same rate in the furnace atmosphere.

After sintering, sample densities were determined by the water immersion technique. The microstructures of the samples were studied by scanning electron microscopy (SEM) equipped with an energy dispersive X-ray spectrometer (EDS) attachment, on polished and thermally etched surfaces. The characterization of the microstructure is an important step in this type of sintered bodies. The densification characteristics were examined in terms of the physical and chemical nature of structures through the change in porosity, second phase formations and distributions and grain growth. Vickers microhardness values were measured with a Leitz mini load hardness tester by an applied load of 300 g on the polished surface. An average of 10 indentations per specimen were taken. Compositions, the percentage of the theoretical density attained after sintering at 1250°C, 1350, 1450 and 1550°C and the hardness values are tabulated in Tables 1 and 2. Table 3 shows the average grain size values with standard deviations of the samples sintered at different sintering temperatures. Standard line intercept techniques were used to determine these values.

3 RESULTS AND DISCUSSION

The microstructures of samples sintered at given temperatures are shown in the scanning electron micrographs given in Figs 1–6. The sintered densities of the samples with MnO_2 and TiO_2 additions ranged between 95 and 98% of the theoretical densities attained at temperatures as low as 1250°C with high hardness values of around 2300 kg mm^{-2}.

The effect of additives on the densification characteristics of alumina is primarily sensitive to the processing conditions, such as the origin of starting powders, amount of additives, blending and mixing techniques, compaction and sintering conditions. Experiments on the undoped samples that were sintered at 1250–1550°C exhibited the typical densification behaviour in agreement with the previous studies showing that a complete sintering can be achieved above 1550°C.[16] The data and the microstructure of the undoped samples are presented for the purpose of comparison (Fig. 1(a)–(d).

The samples with 3 wt% MnO_2 additions exhibited significant difference in densification and measured hardness values. As seen in Fig. 2(a)–(d), considerable densification was already achieved at 1350°C; however, higher densities seem to be attained at 1450°C with an average grain size of 1.66 μm. EDX-point analysis from the large size particles shown in Fig. 7 indicates that MnO_2 enters the solid solution with alumina. An exaggerated and inhomogeneous grain growth with a high amount of pores trapped and clustered within the grains was observed in samples sintered at 1550°C. Mn–Ca rich glassy phase and a wide variety of precipitate morphology due to Ca segregation are evident in these samples. Draining of second phase and its needle-like appearance coming out of grain boundaries indicate that oversintering occurred at this temperature. Such an

Table 1. Compositions and percent of the theoretical densities (%) attained after sintering of the samples at different temperatures (°C)

Sample	1250	1350	1450	1550
A—Undoped	68.7	77.1	89.9	95.0
B—3.0 wt% MnO_2	73.0	86.3	96.2	98.7
C—3.0 wt% TiO_2	81.1	95.0	95.2	97.5
D—3.0 wt% MnO_2-0.5 wt% TiO_2	98.2	98.2	98.5	98.5
E—3.0 wt% MnO_2-1.5 wt% TiO_2	94.4	98.2	98.2	95.9
F—3.0 wt% MnO_2-3.0 wt% TiO_2	98.2	98.5	95.0	95.2

Table 2. Vickers Microhardness (kg/mm^2) of the samples sintered at different temperatures (°C)

Sample	1250	1350	1450	1550
A—Undoped	–	1860±160	2100±130	2300±196
B—3.0 wt% MnO_2	–	1960±208	2190±215	2530±273
C—3.0 wt% TiO_2	–	2390±307	2220±143	2360±375
D—3.0 wt% MnO_2-0.5 wt% TiO_2	2360±151	2430±226	1990±140	1860±182
E—3.0 wt% MnO_2-1.5 wt% TiO_2	2250±95	2230±149	2270±241	2530±252
F—3.0 wt% MnO_2-3.0 wt% TiO_2	2200±255	2280±205	2080±210	2730±211

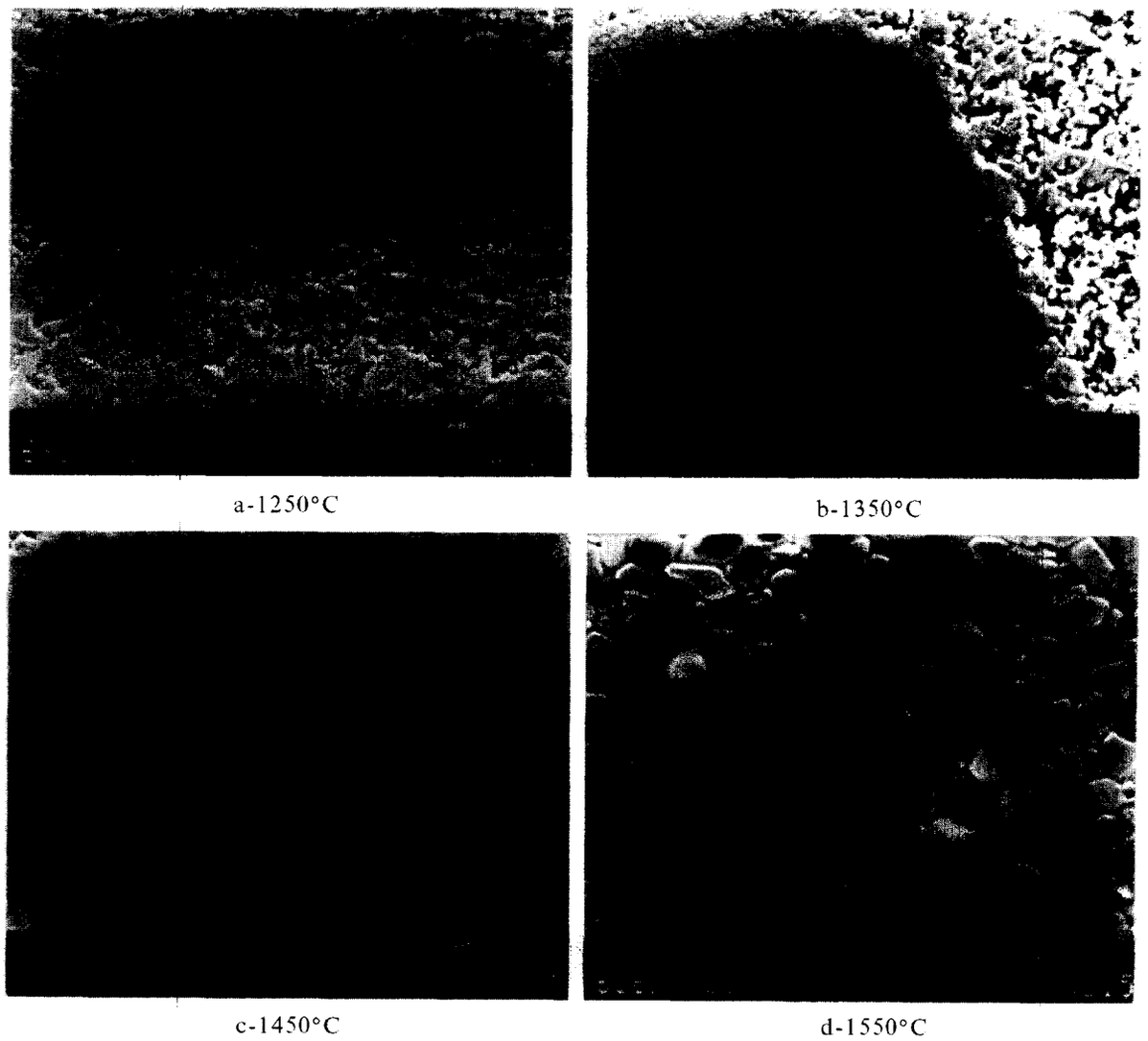

Fig. 1. (a)–(d) Microstructures of undoped alumina samples sintered at 1250, 1350, 1450, and 1550°C.

Table 3. Average grain size values (μm) for the samples sintered at different temperatures (°C)

Sample	1250	1350	1450	1550
A—Undoped	~0.32	~0.33	0.84±0.04	1.48±0.25
B—3.0 wt% MnO_2	~0.51	0.84±0.03	1.66±0.14	12.87±10.23
C—3.0 wt% TiO_2	~0.82	1.47±0.33	2.32±0.46	7.05±2.62
D—3.0 wt% MnO_2-0.5 wt% TiO_2	1.21±0.10	3.01±0.51	5.42±1.53	9.15±5.50
E—3.0 wt% MnO_2-1.5 wt% TiO_2	1.27±0.28	3.33±1.40	8.99±4.10	21.96±2.25
F—3.0 wt% MnO_2-3.0 wt% TiO_2	1.35±0.06	6.57±3.11	18.67±15.8	12.40±13.24

observation correlates well with the eutectic in MnO_2–Al_2O_3 system.[17] The EDX-ray spectrum of this sample shown in Fig. 8 shows strong Mn and Ca peaks together with an Al peak (probably arises from the Al-rich matrix). In one of the recent studies, a second phase formation between the grains was reported in the case of the addition of 0.5–1.5 wt% MnO_2 to alumina since the solid solubility of MnO_2 in alumina is very limited. A eutectic composition present in the MnO_2-rich side of the binary MnO_2–Al_2O_3 system at 1520°C also may indicate the formation of a fragmentary liquid phase at 1550°C.[18]

A 3 wt% TiO_2 addition has also led to a significant increase in hardness to 2390 kg mm^{-2} at temperatures of 1350°C and above. Microstructural features shown in Fig. 3(a)–(d) also indicate that the densification started at 1250°C, and 95% of the theoretical density was already achieved at 1350°C. A high amount of pore formation in between the small and large grains and inhomogeneous grain growth are evident in these compositions. An

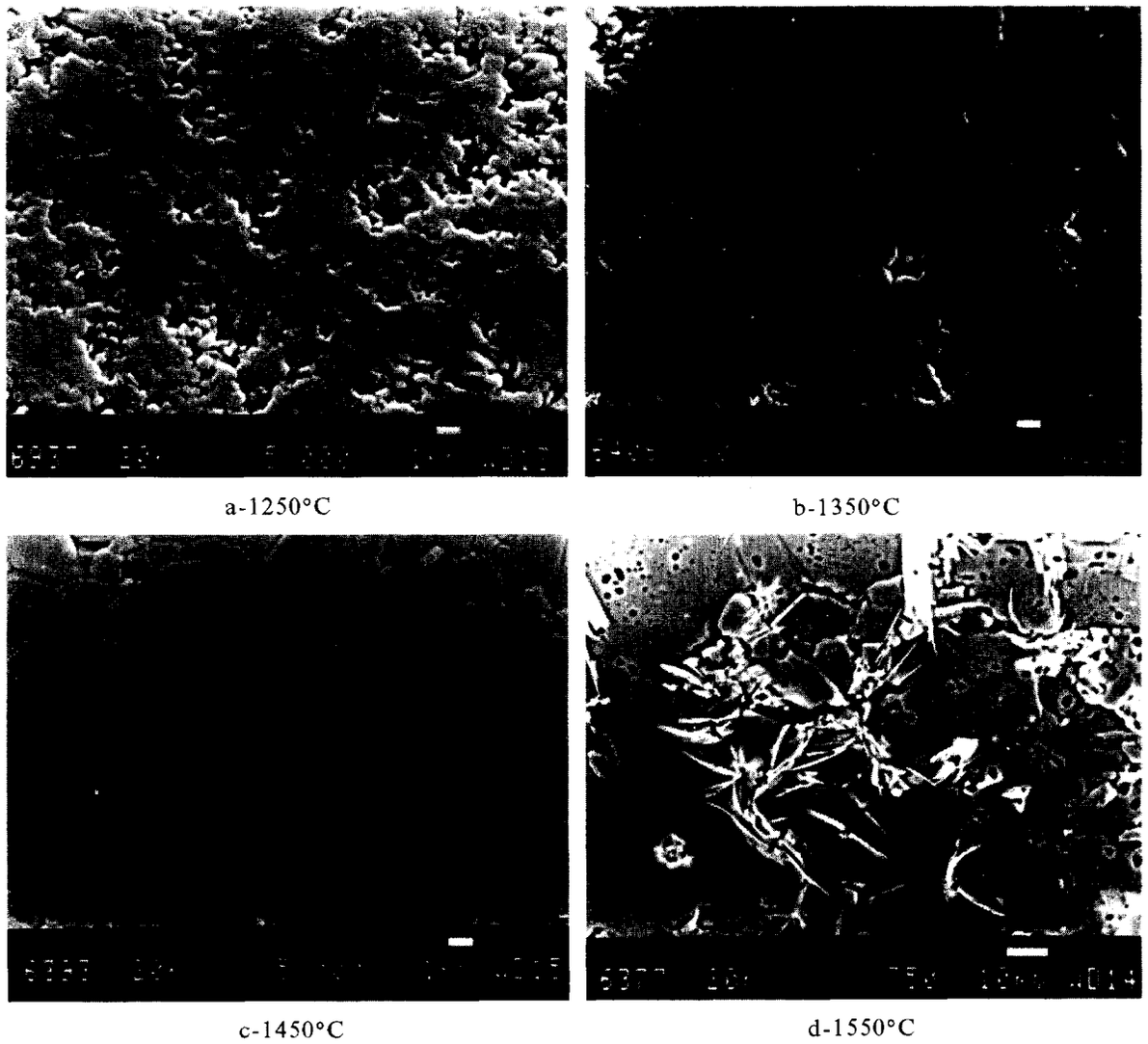

a-1250°C b-1350°C

c-1450°C d-1550°C

Fig. 2. (a)–(d) Microstructures of Al_2O_3-wt% MnO_2 samples sintered at 1250, 1350, 1450, and 1550°C.

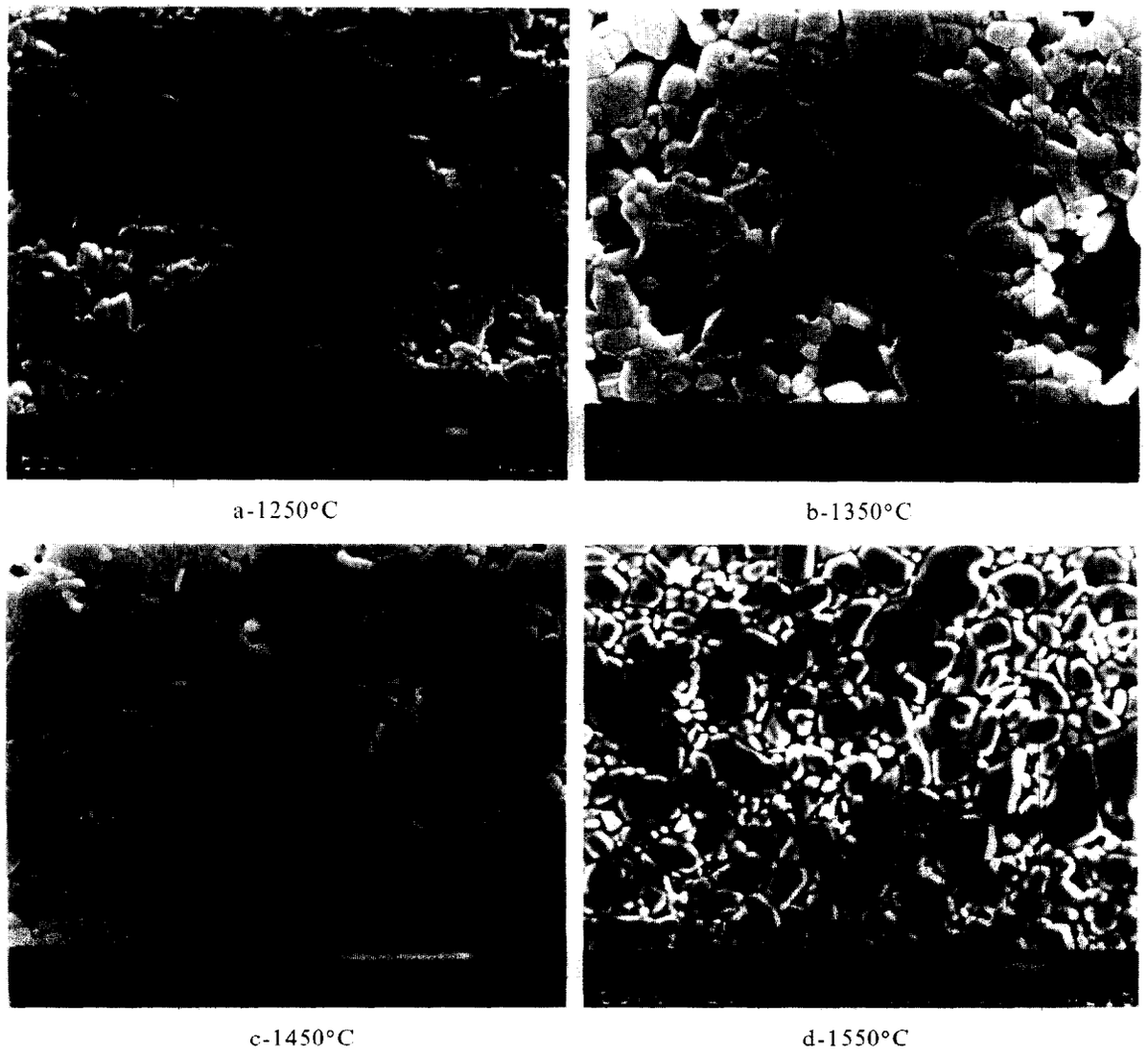

Fig. 3. (a)–(d) Microstructures of Al_2O_3-wt% TiO_2 samples sintered at 1250, 1350, 1450, and 1550°C.

irregular second phase particle distribution is also observed at 1450°C. TiO_2 addition has promoted the grain growth more effectively compared to that of MnO_2 addition; however, the grain growth in the samples sintered at 1350 and 1450°C was found to be inhomogeneous. Ti-rich second phase particles can be distinguished with their white-coloured appearance in the samples sintered at 1450°C (Fig. 9). Excessive grain growth (average 7.05 μm) is also apparent at 1550°C, although a more homogeneous grain size distribution together with second phases in fine granular form and a high amount of intergranular pores are the typical features in these samples.

Compared to single MnO_2 or TiO_2 doping, considerably higher densifications (95–98% of the theoretical densities) in samples with MnO_2 and TiO_2 addition were attained at 1250°C with high hardness values in the range of 2200–2360 kg mm^{-2}. The microstructure of the samples sintered at 1250°C shows a faceted stable grain configuration with average sizes, 1.21–1.35 μm. At 1350°C, higher densifications (98.2–98.5 of the theoretical densities) and some grain growth with an average size of 3.01–6.57 μm are evident in the microstructures with the second phase particles in between the grains (Figs 4(a), 5(a) and 6(a)). Draining of the liquid phase was observed in samples with 3 wt% MnO_2–0.5 wt% TiO_2 additions which were sintered at 1350°C exhibiting crystallized thin needle-like second phase forms distributed evenly throughout the microstructure (Fig. 4(b)–(d)).

The microstructure of samples sintered at 1450 and 1550°C presents extensive and exagerrated grain growth (average 5.42–21.96 μm) with high hardness values in the range of 1860–2730 kg mm^{-2}. In Fig. 4(d) (with 3 wt% MnO_2-0.5 wt% TiO_2 addition, sintered at 1550°C), there seems to be extensive draining of the second phase, presumably liquid during some stage of the densification, coming out of the grains and sweeping over the structure. This phase is rich in Mn–Ti and contains

Al_2O_3 as well, indicating that interface reactions took place during the sintering (Fig. 10). In the samples sintered at 1550°C with 3 wt% MnO_2-1.5 wt% TiO_2 addition, the liquid phase seems to penetrate the grain boundaries and distributed itself evenly through the grains (Fig. 5(d)). The EDX-ray spectrum of grain boundary area given in Fig. 11 shows the existence of Mn- and Ti-rich intergranular glassy liquid phase. A more homogeneous microstructure seems to prevail because of the effect of a liquid intergranular phase along which the grains can rearrange themselves and

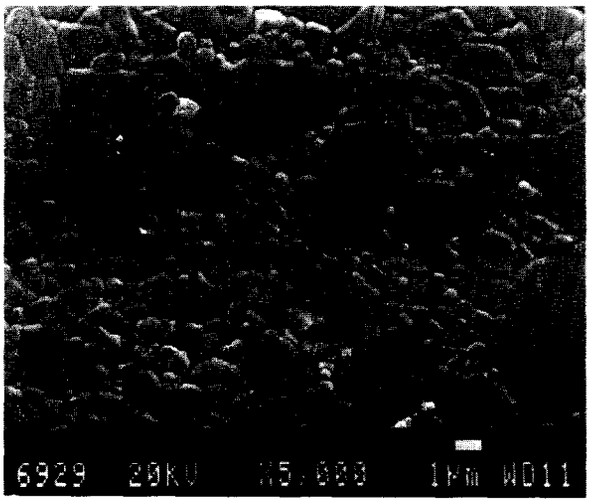

a-1250°C

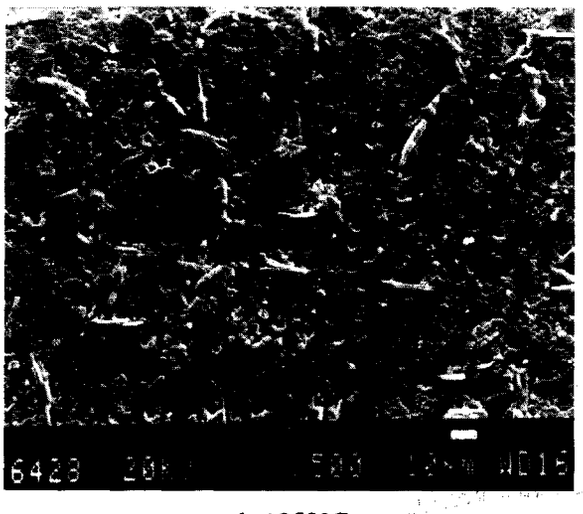

b-1350°C

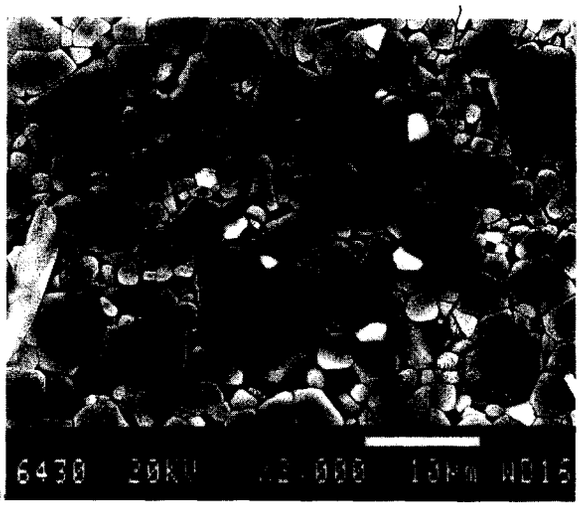

b-1350°C

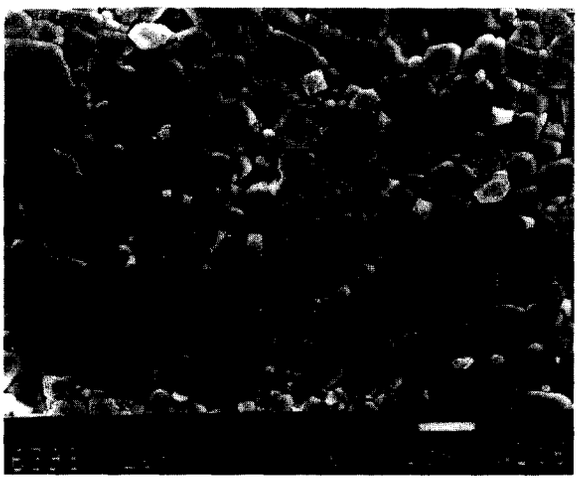

c-1450°C

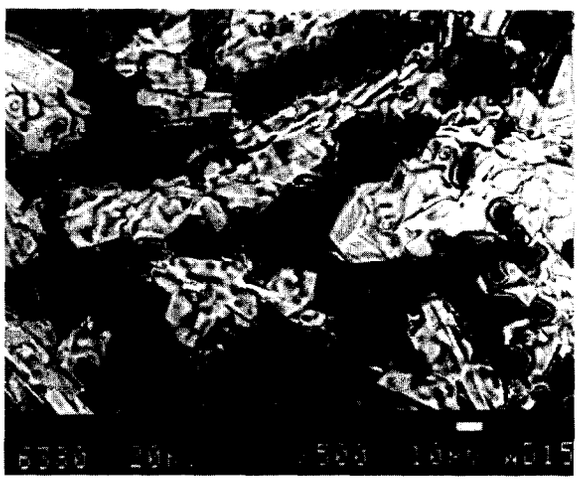

d-1550°C

Fig. 4. (a)–(d) Microstructures of Al_2O_3-wt% MnO_2-0.5 wt% TiO_2 samples sintered at 1250, 1350, 1450, and 1550°C.

form equiaxed shapes. The solution-precipitation mechanism is also enhanced through this phase and intensifies grain growth.

In the microstructures given in Fig. 6(a)–(d) (3 wt% MnO_2-3 wt% TiO_2), an exaggerated but homogeneous grain growth is also evident for the samples sintered at 1450°C, but the second phase distribution seems to be uneven throughout the structure. Presumably, glassy phase pockets form along grain boundaries and also in grain junctions.

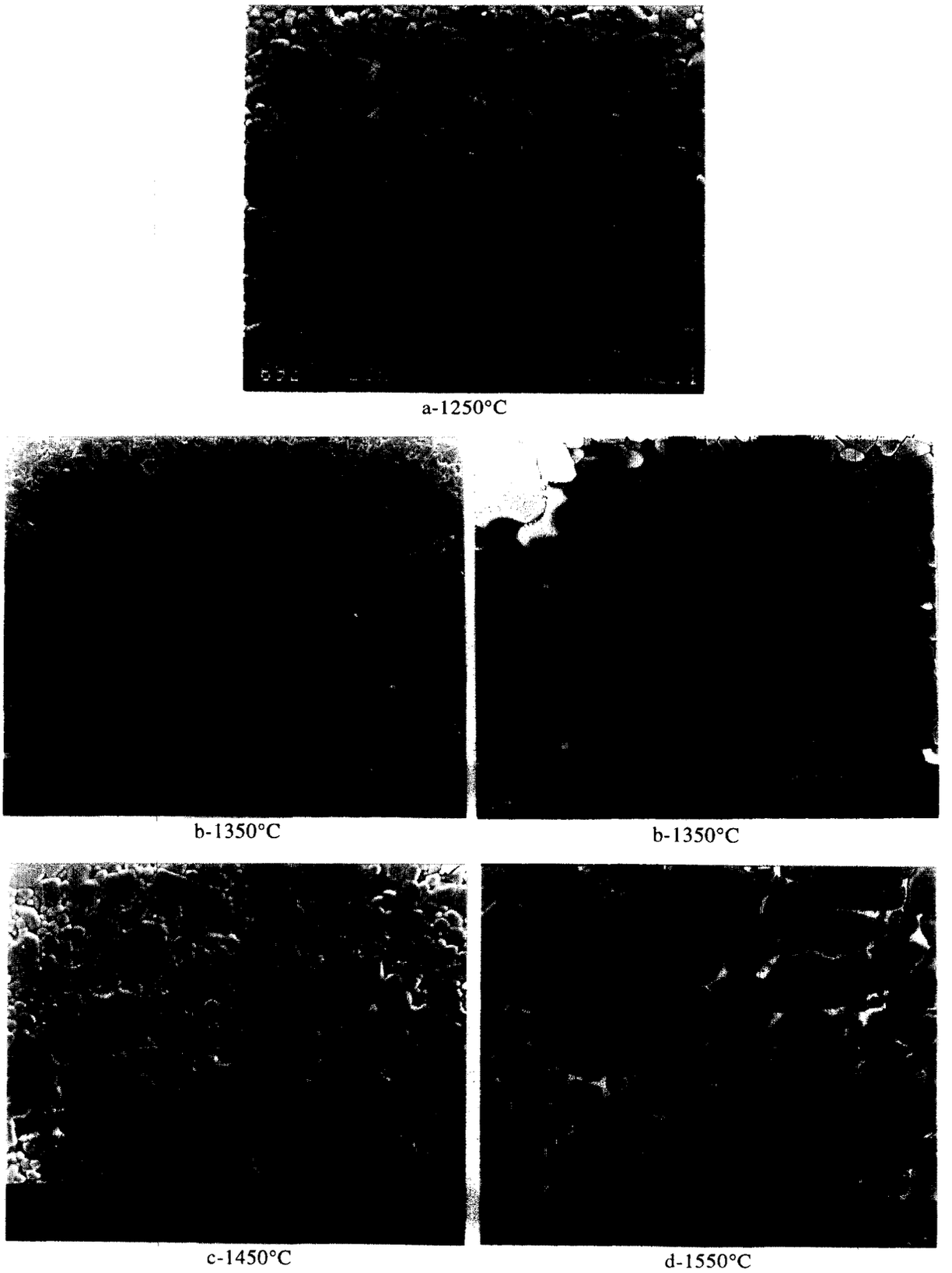

Fig. 5. (a)–(d) Microstructures of Al_2O_3-wt% MnO_2-1.5 wt% TiO_2 samples sintered at 1250, 1350, 1450, and 1550°C.

4 CONCLUSION

The densification and microstructural development of Al_2O_3 with MnO_2 and TiO_2 additions both separately and together were characterized by their promotion to the grain growth and lowering of the sintering temperatures. When MnO_2 and TiO_2 were added together to alumina, a high

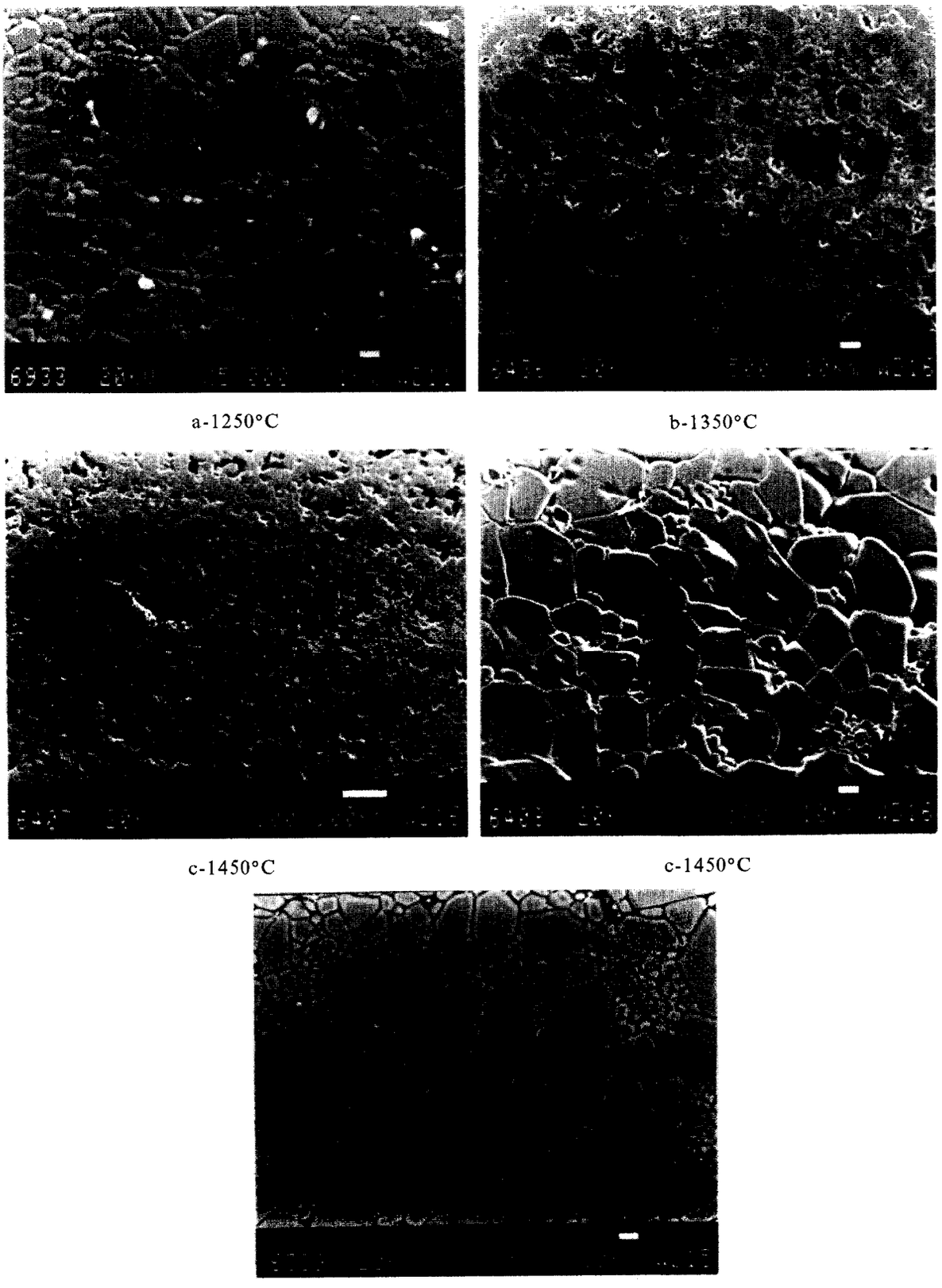

a-1250°C b-1350°C

c-1450°C c-1450°C

d-1550°C

Fig. 6. (a)–(d) Microstructures of Al_2O_3-wt% MnO_2-wt% TiO_2 samples sintered at 1250, 1350, 1450, and 1550°C.

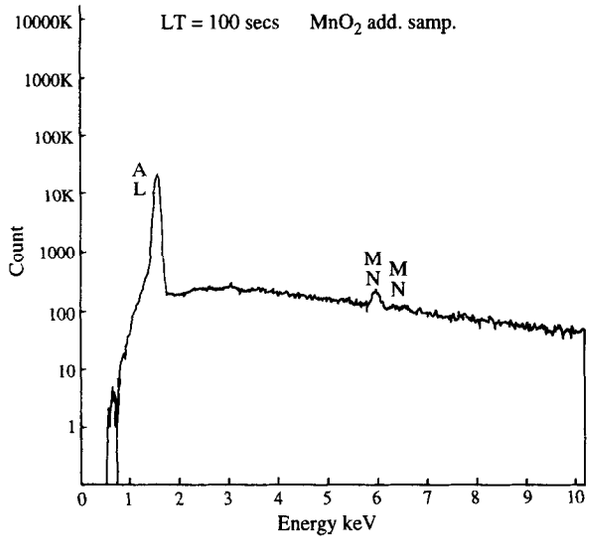

Fig. 7. EDX-point analysis from a large size particle of Al_2O_3-wt% MnO_2 samples.

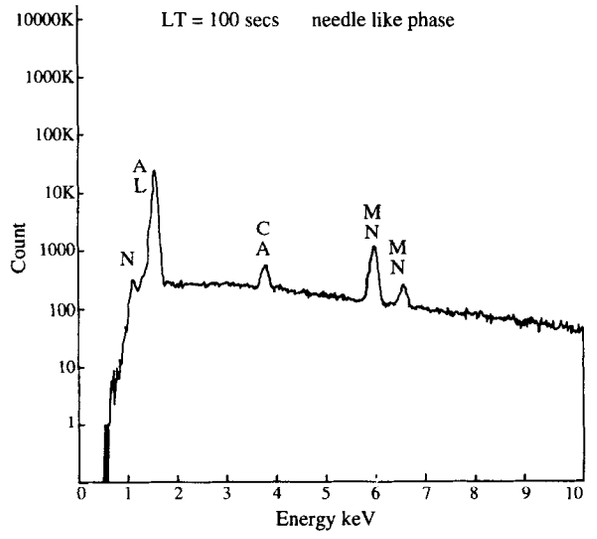

Fig. 8. EDX-ray spectrum of the second phase formation in Al_2O_3-wt% MnO_2 sample.

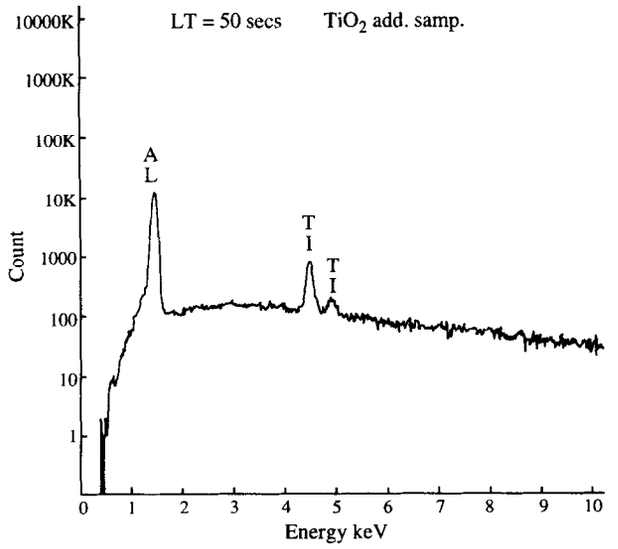

Fig. 9. EDX-ray spectrum of Al_2O_3-wt% TiO_2 sample.

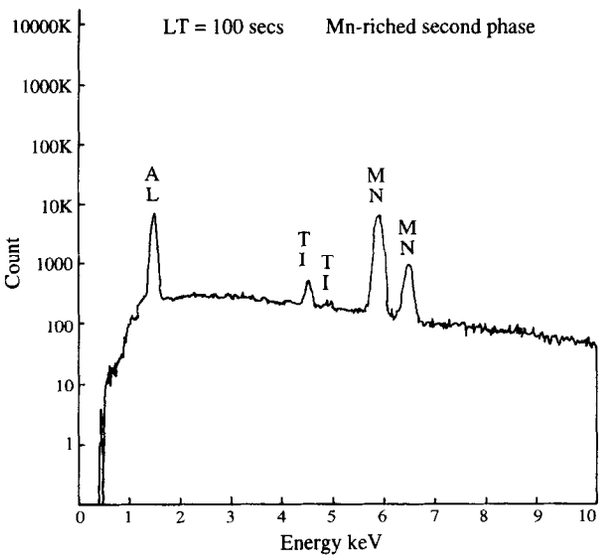

Fig. 10. EDX-ray spectrum of the Mn-rich second phase formation in Al_2O_3-wt% MnO_2-0.5 wt% TiO_2 samples sintered at 1550°C.

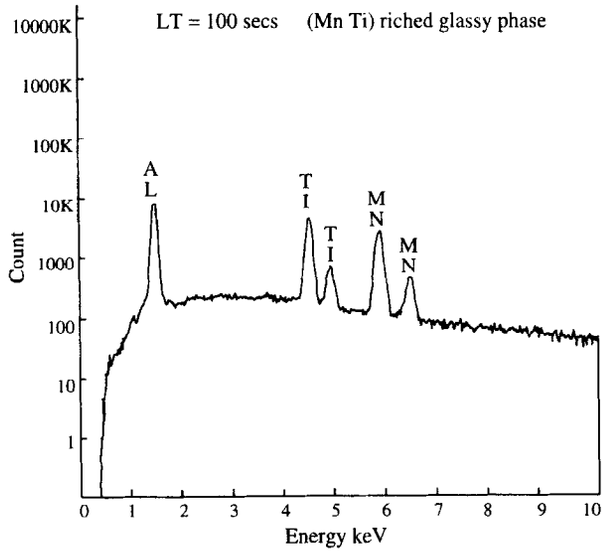

Fig. 11. EDX-ray spectrum of the grain boundary area in Al_2O_3-wt% MnO_2-1.5 wt% TiO_2 sample sintered at 1550°C.

densification up to 98.2% of the theoretical density was attained at temperatures as low as 1250°C. Microhardness measurements of alumina compositions with MnO_2 and TiO_2 additions reveal high hardness values in contrast with high sintered densities. Second phase precipitation with various morphologies and intergranular liquid phase formation along with extensive grain growth were also observed in Al_2O_3–MnO_2–TiO_2 system, which were sintered at higher temperatures.

ACKNOWLEDGEMENTS

The authors acknowledge the financial support of NATO-SFS Programme for this study. The

authors also thank to R. Isık and O. Ipek for their valuable help during the study.

REFERENCES

1. BROOK, R. J., HOWLETT, S. P. & SU XING WU, In *Sintering—Theory and Practice*. Elsevier, The Netherlands, 1982, p. 135.
2. SUMITA, S., *J. Ceram. Soc. Japan, Int. Ed.*, **99**(7) (1991) 525.
3. XUE, L. A. & CHEN, I. W., *J. Am. Ceram. Soc.*, **74**(8) (1991) 2011.
4. ROSSI, G. & BURKE, J. E., *J. Am. Ceram. Soc.*, **56**(12) (1973) 654.
5. CAHOON, H. P. & CHRISTENSEN, C. J., *J. Am. Ceram. Soc.*, **39**(10) (1956) 337.
6. MCKEE, W. D. & ALESHIN, E., *J. Am. Ceram. Soc.*, **46**(1) (1963) 54.
7. HARMER, M., ROBERTS, E. W. & BROOK, R. J., *Trans. Br. Ceram. Soc.*, **18**(1) (1979) 22–25.
8. ROY, S. K. & COBLE, R. L., *J. Am. Ceram. Soc.*, **51**(1) (1968) 1.
9. SMOTHERS, W. J. & REYNOLDS, H. J., *J. Am. Ceram. Soc.*, **37**(12) (1954) 588.
10. BAGLEY, R. D., CUTLER, I. B. & JOHNSON, D. L., *J. Am. Ceram. Soc.*, **53**(3) (1970) 136.
11. KESKI, J. R. & CUTLER, I. B., *J. Am. Ceram. Soc.*, **48**(12) (1965) 653.
12. KESKI, J. R. & CUTLER, I. B., *J. Am. Ceram. Soc.*, **51**(8) (1968) 440.
13. RABE, T., NOBST, P., MOSER, B. & KOHNKE, K., *Silikattechnik*, **34** (1983) 49.
14. CUTLER, J., BRADSHAW, C. & HYATT, E., *J. Am. Ceram. Soc.*, **40**(4) (1957) 134.
15. KOSTIC, E., KISS, S. J. & BOSKOVIC, S., *Pow. Met. Int.*, **22**(2) (1990) 29.
16. ALCOA Chemicals Division Product Data (Aluminium Company of America, 1501 Pittsburg, PA 15219).
17. LEVIN, E. M., ROBBINS, C. R., MCMURDIE, H. F. & RESER, M. K., (eds), In *Phase Diagrams For Ceramics*, 4th edn. American Ceramic Society, 1979, p. 114.
18. ERKALFA, H., MISIRLI, Z., BAYKARA, T., DOGAN, F. & AKSAY, I. A., *Third Euro-Ceramics*, Vol. 3. Faenza Editrice, Spain, 1993, p. 549.